Title

Long read sequencing identifies complex structural variant landscape and recurrent TERT rearrangements in mucoepidermoid carcinoma.

Authors

Gensterblum-Miller, Elizabeth

Bhangale, Apurva

Majid, Dana

et al.

Publication Date

2024-12-01

DOI

10.1016/j.oraloncology.2024.107108

Peer reviewed

HHS Public Access

Author manuscript

Oral Oncol. Author manuscript; available in PMC 2025 April 10.

Published in final edited form as:

Oral Oncol. 2024 December ; 159: 107108. doi:10.1016/j.oraloncology.2024.107108.

Long read sequencing identifies complex structural variant landscape and recurrent TERT rearrangements in Mucoepidermoid Carcinoma

Elizabeth Gensterblum-Miller[1,2], **Apurva Bhangale**[1], **Dana Al Majid**[1], **Victor Murcia Pienkowski**[3], **Malgorzata Rydzanicz**[3], **Joanna Janiszewska**[4], **Magdalena Kostrzewska-Poczekaj**[4], **Clifford Chang**[1], **Collin Brummel**[1], **Nicole L. Michmerhuizen**[1,5], **Jiayu Wang**[1,5], **Erin Sandford**[6], **Muneesh Tewari**[6,8], **Malgorzata Wierzbicka**[4], **Andrew C. Birkeland**[1], **Jonathan B McHugh**[7,8], **Matthew E. Spector**[1,8], **Maciej Giefing**[4], **Malgorzata Jarmuz-Szymczak**[4], **Molly E Heft Neal**[1], **J. Chad Brenner**[1,2,5,8,†]

[1]Department of Otolaryngology – Head and Neck Surgery, University of Michigan, Ann Arbor, MI.

[2]Cellular and Molecular Biology Program, University of Michigan, Ann Arbor, MI.

[3]Department of Medical Genetics, Medical University of Warsaw, Warsaw, Poland

[4]Institute of Human Genetics, Polish Academy of Sciences, Poznan, Poland.

[5]Department of Pharmacology, University of Michigan, Ann Arbor, MI.

[6]Department of Int Med-Hematology/Oncology, University of Michigan, Ann Arbor, MI.

[7]Department of Pathology, University of Michigan, Ann Arbor, MI.

[8]Rogel Cancer Center, University of Michigan, Ann Arbor, MI.

Abstract

Mucoepidermoid Carcinoma (MEC) is a common salivary malignant neoplasm. Approximately 60% of MECs harbor translocations between *CRTC1* or *CRTC3* and *MAML2*, which are thought to drive disease pathogenesis. However, the precise structural mechanism driving this

[†]Corresponding Author J. Chad Brenner, PhD, 1500 E. Medical Center Dr. 9301B MSRB3, Ann Arbor, MI 48109.

Author Contributions

CRediT Classification:

Conceptualization: Chad Brenner

Data curation: Molly Heft Neal, Apurva Bhangale, Elizabeth Gensterblum-Miller, Nicole Michmerhuizen, Dana Al Majid, Clifford Chang, Erin Sandford, Jiayu Wang, Malgorzata Jarmuz-Szymczak, Malgorzata Rydzanicz, Joanna Janiszewska, Magdalena Kostrzewska-Poczekaj, Malgorzata Wierzbicka, Maciej Giefing

Formal analysis: Molly Heft Neal, Apurva Bhangale, Elizabeth Gensterblum-Miller, Muneesh Tewari, Maciej Giefing, Jonathan McHugh, Malgorzata Jarmuz-Szymczak, Victor Murcia Pienkowski, Joanna Janiszewska, Magdalena Kostrzewska-Poczekaj, Matthew Spector, Chad Brenner

Investigation: Molly Heft Neal, Apurva Bhangale, Elizabeth Gensterblum-Miller, Collin Brummel, Nicole Michmerhuizen, Clifford Chang, Maciej Giefing, Jonathan McHugh, Erin Sandford, Jiayu Wang, Malgorzata Jarmuz -Szymczak, Victor Murcia Pienkowski, Joanna Janiszewska, Magdalena Kostrzewska-Poczekaj

Visualization: Elizabeth Gensterblum-Miller, Apurva Bhangale, Molly Heft Neal

Methodology: Chad Brenner

Resources and Supervision: Chad Brenner

Validation: Molly Heft Neal, Apurva Bhangale, Elizabeth Gensterblum-Miller, Nicole Michmerhuizen, Clifford Chang, Malgorzata Jarmuz-Szymczak, Victor Murcia Pienkowski, Maciej Giefing

Writing - original draft: Chad Brenner, Molly Heft Neal, Elizabeth Gensterblum-Miller

Writing - review and editing: All authors

rearrangement remains uncharacterized. Here, we performed multi-omic and long read genomic sequencing, discovering a chain of alterations that created the *CRTC1::MAML2* fusion, but also an unexpected *MAML2* to *MYBL1* rearrangement, suggesting that *MYBL1* may play a larger role in salivary gland cancers than previously recognized. Furthermore, we discovered and validated recurrent *TERT* rearrangements and amplifications in MEC models. 5/5 MEC cell lines and 36/39 (92%) primary MEC tumors harbored a *TERT* rearrangement or copy number amplification. Custom sequencing of the *TERT* locus confirmed translocation breakpoints in 13/33 (39%) MECs, while exome sequencing confirmed frequent *TERT* amplifications. Critically, *TERT* knockdown in NCI-H292, a cell line with *TERT* promoter rearrangement, reduced clonogenic cell survival, supporting a critical role of this gene in MEC tumorigenesis. Overall, our data suggest that complex chromothripsis rearrangement mechanisms drive the formation of structural variation in *CRTC1::MAML2* fusion positive and negative tumors and reveal highly recurrent structural variation driving *TERT* rearrangement in MEC.

Keywords

MEC; translocation; structural variation; *CRTC1* ; *MAML2* ; *NOTCH2* ; *TERT*

Introduction

Mucoepidermoid carcinoma (MEC) is one of the most common salivary malignancies, accounting for 30–40% of salivary gland malignancies in adults and 50% in children[1–3]. The disease commonly occurs in the parotid gland, or occasionally the submandibular and minor salivary glands[4]. MEC is characterized by grades based on histological appearance (low, intermediate, and high grade). The drivers of survival outcomes vary by study and include histological grade, tumor location, tumor stage, nodal status, patient age, margin status, and perineural invasion[2, 3, 5–7].

The molecular landscape of MEC remains largely unknown Recent studies have identified EGFR signaling alterations and rare *TP53* mutations[8–12], but salivary gland cancers, including MEC, are frequently driven by genomic translocations [13]. To date, the only well-described recurrent genetic alteration in MEC is a rearrangement between chromosomes 11 and 19 ((11;19)(q14–21; p12–13)), resulting in the translocation of *CRTC1* and *MAML2*[6, 7, 12, 14–16]. Initially discovered in 2003 by Tonon *et al*, the *CRTC1* to *MAML2* rearrangement was found in 34–88% of MEC cases [10, 12, 16, 17], with a *CRTC3* to *MAML2* rearrangement in a smaller subset of patients [18]. This *CRTC1::MAML2* fusion gene is thought to play a role in tumorigenesis, and several *in vitro* studies have demonstrated that regulating fusion expression also regulates oncogenic phenotypes, possibly through a MYC-and/or CREB-mediated pathway[15, 19–22], or an IGF1-dependent mechanism[23]. Importantly, while initial reports suggested *CRTC1::MAML2* may drive NOTCH pathway reporter activation [14], more recent studies have found that *CTRC1-MAML2* does not affect several common NOTCH signaling effectors[20–22].

While increasing evidence for the prevalence and function of the *CTRC1-MAML2* translocation continues to advance, little is known regarding the genetic mechanism leading to the formation of this translocation. Furthermore, genomic alterations affecting *CRTC1/3::MAML2* negative tumors are an important ongoing problem highlighted in current literature [24].Given these open questions we utilized long read whole genome sequencing approaches to understand the genomic mechanisms driving fusion formation in MEC and to characterize genetic events that contribute to the malignant process.

Materials and Methods

Ethics Statement

This study was approved by two independent ethics boards. The University of Michigan's Institutional Ethical Review Board approved HUM00080561 for genetic analysis of retrospective MEC tissues and cell lines. The study was conducted in accordance with the guidelines of the Declaration of Helsinki and was approved by the Institutional Ethical Review of the University of Medical Sciences 505A/15 (06.05.2015). Demographic information for human subjects is summarized in Table S11. Cell Lines and Reagents

Mucoepidermoid carcinoma NCI-H292 cells were purchased from the American Type Culture Collection (ATCC, Manassas VA, USA) and genotyped throughout the study, as previously described, to confirm their authenticity [25]. Mucoepidermoid carcinoma UM-HMC-1, UM-HMC-3A, and UM-HMC-3B cells were generously provided by Dr. Jacques Nör from the University of Michigan School of Dentistry [26]. The new MEC cell line IHG-MUC360 was derived and characterized by J. J., M. K., M. W., M. G., and M. J. (Patent No. PAT.229,507, granted by the Polish Patent Office, European Patent Register No. PL229507B1), and deposited in the German Collection of Microorganisms and Cell Cultures GmbH (DSMZ). The sinonasal undifferentiated carcinoma cell line MDA8788–6 was generously provided by M.D. Anderson and was generated as previously described by Takahashi *et al* [27]. The oral cavity cell lines UMSCC-47 and UMSCC-104 were selected from our head and neck repository [28]. IHG-MUC360 was cultured in DMEM containing 2 mM L-glutamine, 1% Non-Essential Amino Acids, 20% FBS, 5 mg/L insulin, 5×10–5 M hydrocortisone, 100 U/mL penicillin, and 100 g/mL streptomycin. All other cell lines were grown exponentially in DMEM (UM-HMC-1, UM-HMC-3A, UM-HMC-3B, UMSCC-47, UMSCC-104, and MDA8788–6) or RPMI (NCI-H292) containing 10% FBS, 7μg/mL penicillin/streptomycin and 1% non-essential amino acids. Media used to grow UM-HMC-1, 3A, and 3B was further supplemented with hydrocortisone (400ng/mL), EGF (20ng/mL), and insulin (5μg/mL). PDX models were obtained from the NCI Patient-Derived Models Repository (PDMR) (NCI-Frederick, Frederick National Laboratory for Cancer Research, Frederick, MD, USA).

Sequencing and Bioinformatics Methods.

Extended methods are available in the Supplemental Text.

Cell Biology Methods.

Extended methods are available in the Supplemental Text.

Statistical Analysis

Telomere length was compared using Student's t-test. A p-value <0.05 was considered statistically significant. Statistical analyses were performed using Prism v8 (GraphPad Software, San Diego, CA, USA).

Results

Nanopore Long Read Sequencing and Linked Read Sequencing Identifies Novel Rearrangements:

We first sought to characterize the *CRTC1::MAML2* breakpoint sequence of MEC-derived cell lines NCI-H292, UM-HMC-1, UM-HMC-3A, and UM-HMC-3B (Figure 1), using Nanopore long-read sequencing of high molecular weight DNA. These generated 617,700–4,130,516 reads with an average length of 6,122.4–8,705.1 nucleotides (Table S1 and Figure S1). For each cell line, we identified multiple reads directly spanning the *CRTC1* and *MAML2* fusion (Figure 1A) and determined the location and sequence of the *CRTC1::MAML2* breakpoint (Figure 1B-D). As expected, the translocation breakpoint varied for each cell line, though it always occurred in the first intron of *CRTC1* and *MAML2*. UM-HMC-3A is derived from a local recurrence, and UM-HMC-3B is derived from a recurrent metastatic lesion from the same patient. As anticipated, both cell lines contained the same *CRTC1::MAML2* breakpoint sequence [26].

We performed linked read genome-wide sequencing of the *CRTC1::MAML2* fusion-positive NCI-H292 cell line. Following 10x-based linked read barcoding of high molecular weight DNA, we generated 913,409,176 sequencing reads. 95.90% mapped the reference genome, with a mean genome depth of 39.8X (Table S4). 93.4% of the sequenced molecules were greater than 20 kb in length and 18.8% were greater than 100 kb in length. From this dataset, 99.5% of SNPs were phased across the genome, with phase blocks up to 39,295,952 bp in length, supporting a high-quality linked read genome dataset. In-depth analysis of the genome identified 139 large structural variations. Most of these alterations were deletions or duplications, ranging in length from 20 kb to 1–2 Mb (Table S5), from which we identified nine high-confidence chromosomal rearrangements, including *CRCT1-MAML2* translocation (Figure 2A-C; Table S5). While the linked read data identified the *CRTC1::MAML2* rearrangement, we did not identify any reads spanning the *CRTC1::MAML2* junction, potentially due to the high GC content and low read representation of *CRTC1* intron 1. We did, however, successfully identify translocation events associated with *CRTC1::MAML2* formation.

In NCI-H292 cells, the *CRTC1::MAML2* translocation occurred through a series of five genomic events consisting of four linked translocations and one genomic deletion. Unique reads were used to map the breakpoints to Chr19:18,794,730 in *CRTC1* and Chr11:95,834,323 in *MAML2* (genome build hg19). Of these genomic events, *CRTC1* Chr19:18,795,369 was translocated adjacent to *SGK3* Chr8:67,777,508, and the 3' end of the breakpoint at Chr8:67,777,554 was translocated to Chr6:75,131,786 in *RP11554D151*. Furthermore, the 5' end of *MAML2* was translocated from Chr11:95,834,411 to Chr8:67,527,412, which resides between *VCPIP1* and *MYBL1*, and was also associated

with a deletion between Chr8:46,880,000–67,530,000, which contains the *MYBL1* gene (Figures 2A and 2B). Nanopore sequencing confirmed the breakpoint structures between *MYBL1* and *MAML2*, which contained three-nucleotide microhomology at the breakpoint, as well as *SGK3* and *CRTC1,* which had five-nucleotide microhomology at the breakpoint (Figure 2D).

Sanger sequencing was used to confirm the novel translocation junctions between *MYBL1* and *MAML2* as well as *SGK3* and *CRTC1* (Figure S3A and B, Table S6). Sanger sequencing also validated *CRTC1* and *MAML2*, joined by a 3-nucleotide microhomology (Figure S3C). In addition, we validated the *CRTC1::MAML2* translocation in UM-HMC-1 (Figure S3D). Collectively, these data support chromothripsis as a mechanism of rearrangement [29] mediated by a microhomology-driven repair process that leads to the formation of canonical *CRTC1::MAML2* rearrangement in this disease.

Subsequent analysis of additional chromosomal rearrangements in NCI-H292 linked read data revealed a second rearrangement containing over eight linked events, including a promoter rearrangement upstream of *TERT* (Figure 3A). We did not identify supporting nanopore reads for this translocation; therefore, this rearrangement junction was validated by Sanger sequencing. The *PPP2R1B::TERT* junction was found to have no additional insertion nucleotides at the breakpoint and no obvious homology at the junction, suggesting that the rearrangement may have occurred through a different end-joining-based mechanism (Figure 3B).

Given the potential functional importance of this translocation, we next sought to confirm *TERT* promoter rearrangement using a break-apart probe targeting the 5’ and 3’ regions adjacent to *TERT*. We then quantified the *TERT* copy number in each cell by counting the 3’-binding probe, 5’- binding probe, and both overlapping. This revealed a high degree of heterogeneity within each cell line, although the prevalence of each genotype varied between cell lines (Figure 3C). In NCI-H292, 77% of all counted cells demonstrated copy gain of the 3’-binding probe relative to the 5’- binding probe, consistent with the presence of genomic rearrangement (Figure 3C). Cells with a *TERT* copy number greater than 2 were highly enriched in UM-HMC-1 and UM-HMC-3B, but not UM-HMC-3A (Figure 3C). This finding was validated by genome-wide copy number alterations detected by Oncoscan copy number arrays (Figure S4). Using this method, UM-HMC-1 and UM-HMC-3B were found to have an average of three copies of the *TERT* gene per cell, while UM-HMC-3A contained two copies. We further confirmed *TERT* copy gain by digital droplet PCR in NCI-H292 cells relative to normal human reference genomic DNA (Figure S5). Taken together, these copy number analyses support *TERT* amplification in three of four cell lines tested, while demonstrating a 3’ region translocation inNCI-H292.

Further evaluation of the *PPP2R1B::TERT* rearrangement revealed movement of the promoter and 5’ region of *PPP2R1B* from chr11:111,600,986 to chr5:1,296,648, which sits immediately prior to the *TERT* gene. This rearrangement was associated with several additional structural variations in chr11, including multiple deletions and duplications in *UBASH3B*, *ARHGAP32*, and the *BARX2* promoter. This chained structural variation included a rearrangement translocation from *ARHGAP3* chr11:128,920,000 to

a region downstream of *SHFM1* at chr7:134,940,000. The coordinates of the associated rearrangements and a schematic representation are shown in Figure 3D and 3E.

A newly derived *CRTC1::MAML2* fusion-positive MEC model, IHG-MUC360, was also sequenced to narrow the breakpoints of translocation t(5;7)(p15;q34), revealed by cytogenetic analysis, potentially involving the *TERT* gene. For this sample, 32,567,275 read pairs were generated and mapped to the reference genome (hg19). Based on 16 discordant reads (the first read of the pair maps to chromosome 5 and the second maps to chromosome 7), we identified the genomic localization of the translocation, which is presented according to the current nomenclature [30]. For chr(5): t(5;7)(p15;q32)dn.seq[GRCh37/hg19]t(5;7)(7qter→7q32(138,444,233)::5p15(1 302,991)→5qter).

For chr(7):t(5;7)(p15;q32)dn.seq[GRCh37/hg19]t(5;7)(7pter→7q32(138,444,235)::5p15(1 302,889) →5pter). The breakpoint on chromosome 5 is located on a non-coding region approximately 8 kb upstream of the *TERT* gene, whereas the breakpoint on chromosome 7 disrupts *ATP6V0A4* gene (MIM: 605239) in intron 8. (Figure 3F, Table S6) These data show novel translocations involving *TERT* and suggest potential mechanisms of tumorigenesis in MEC.

To explore the functional role of these fusions, we next performed transcribed fusion detection, using RNA sequencing data from NCI-H292, UM-HMC-1, UM-HMC-3A, and UM-HMC-3B cells (Table S7, Table S8). We validated the *CRTC1::MAML2* fusion in each cell line, with 21, 6, 6, and 5 junction-spanning reads. While the *CRTC1::MAML2* translocation DNA sequence differed between cell lines, the sequence of the resulting RNA fusion site remained consistent (Figure S6A). In addition, we detected a *TERT* fusion event in one of the four cell lines sequenced, H292 (Figure S6B). We detected two high-confidence in-frame *PPP2R1B::TERT* transcripts with alternate splicing patterns at the fusion breakpoint.

Determining TERT alteration frequency in primary tumors

Due to the high frequency of *TERT* alterations and evidence of actively transcribed *TERT* fusion in MEC cell lines, we explored TERT alterations in primary tumors. We developed a tissue microarray (TMA) of FFPE-preserved tissue from 61 primary tumors. We performed DNA FISH to detect *TERT* and *MAML2* translocations, using the break-apart system previously described. We then quantified the frequency of samples containing *MAML2* translocation or *TERT* amplification or translocation, including 5'- or 3'-specific alterations (Figure 4A). We found 64% of primary tumors contained a *MAML2* translocation, consistent with translocation rates from previous studies (Figure 4B) [31, 32]. Moreover, one or more types of *TERT* structural variations were detected in 92.3% of all tested tumors (36/39) (Figure 4B). Within each *TERT*-altered tumor, 12.8% +/− 1.4% of all cells contained a *TERT* variation (mean +/− SE, range: 3.2%−35.2%). Interestingly, *TERT* structural variation was significantly associated with *MAML2* translocation-positive tumors (Figure 4C, Fisher's Exact Test, p=0.0283). Of all *TERT*-altered tumors, 73.4% also contained *MAML2* break-apart alterations, and 100% of all MAML2-altered tumors had some form of *TERT* structural variation.

Next, we investigated the correlation between *MAML2* or *TERT* translocation and patient survival. The five-year overall survival rate for this cohort was 87.9% and the five-year disease specific survival rate was 91.4%. Survival was then evaluated using Kaplan-Meier, stratifying by *MAML2* translocation status (Figure 4D). While previously published data show mixed results on the prognostic significance of *MAML2* translocation [7, 33], in our data, the presence of *MAML2* translocation was significantly associated with improved five-year overall and disease-specific survival (p=0.028 and 0.027, respectively). We evaluated the presence of *TERT* translocations on survival, observing a trend towards improved overall survival in the *TERT* translocation-positive patients compared to *TERT* translocation-negative (100% vs. 80.6%, 95% CI for *TERT* negative 61.9–90.8%, p=0.058). The difference was not statistically significant. Tumor grade was significantly associated with five-year disease specific survival (p=0.01). After controlling for tumor grade and *MAML2* mutation using a multivariate Cox regression survival analysis, *TERT* translocation status was not significantly associated with survival (p=0.98). In addition, *TERT* status did not correlate with any clinical variables, including sex, reported race, disease status, grade, or *MAML2* status (Table S10).

To define the *TERT* rearrangement breakpoint locations, we performed targeted capture sequencing (TCS) on 33 salivary MEC tumors (Table S11). We utilized a custom capture panel, targeting genomic regions with translocations identified by long read sequencing, including *CRTC1*, *MAML2*, *TERT*, *MYBL1*, and *ATP6V0A4* (Table S12). Alignment of paired end short read DNA sequencing resulted in 55.3x average read depth (Table S13).

We then performed structural variant calling on these samples, using the *Dysgu* Python package [34]. After filtering (Supplemental Text), we identified a mean of 2.97 breakpoints per tumor (Figure 5A, Table S14). As expected, *MAML2* and *TERT* locus translocations [chr5:1,153,147–1,395,068] were common in the cohort (Figure 5A, Table S14). We detected *MAML2* translocations in 21/33 (64%) samples, 9 of which included *CRTC1::MAML2* (Figure 5A-C). These *MAML2* breakpoints are exclusively found in intron 1 (Figure 5E) Likewise, we detected *TERT* locus translocation breakpoints in 13/33 (39%) independent tumors. There is significant overlap in samples containing *MAML2* and *TERT* locus translocations (Fisher's exact test, p=0.0005; Figure 5B). Importantly, *TERT* rearrangement partners were tumor-specific, and we did not identify common features of these rearrangement partners, suggesting that the translocated portions of the *TERT* gene are critical for the oncogenic effects (Figure 5D). *TERT* locus breakpoints localized throughout *TERT,* as well as the neighboring genes *SLC6A18* and *SLC6A19* (Figure 5F).

To further explore the molecular landscape of mucoepidermoid carcinoma and the prevalence of *TERT* alterations, we assembled a cohort of tumor samples from patients treated at the University of Michigan (Figure S8A). Eleven samples underwent whole-exome sequencing, with an average of 124,214,959 uniquely mapped reads (83.8%) (Table S15). Using these data, we identified a median mutational burden of 36, with one tumor, MEC001, harboring 1006 mutations, an exceptionally high number (Figure S9A). Microsatellite instability analysis demonstrated that MEC001 was unstable, consistent with the high mutational burden (Table S16). Next, we used these data to determine the HLA type (Table S17) and neoantigen load of each tumor, finding a median predicted neoantigen load of

2.5 (Figure S9B). Overall, 11 samples showed a relatively low total mutational burden, consistent with the high frequency of genomic rearrangements observed in our long read and linked read sequencing data. We then performed molecular signature analysis using the Mutational Patterns pipeline [35], which identified a strong enrichment of COSMIC mutational signature 3 (Figure S8B, C), associated with homologous recombination double-strand break repair deficiencies in breast, ovarian, and pancreatic cancers [36, 37]. The other enriched signatures (5 and 12) had unknown significance at this time [36]. Collectively, exome sequencing data support that MEC tumors may have impaired DNA double-strand break repair, consistent with the enrichment in genomic rearrangements and structural variations observed in linked read data.

We then analyzed specific high-confidence single nucleotide variants and indels, depicted in Figure 4E-F (SNV and INDELs are summarized in Tables S18 and S19, respectively). These include recurrent alterations in *MUC12, MUC3A, MUC4,* and *MUC5B,* a gene family implicated in disease pathogenesis for tumors of the aerodigestive tract [38, 39] and more recently shown to have potential prognostic significance in MEC [40, 41]. Recurrent *NOTCH2* mutational alterations were also found (4/11 tumors), including Cys877Phe in MEC023, predicted to be functionally significant by the VEST functional annotation pipeline ($P < 0.1$, Table S20); a 5'-UTR 3 nucleotide deletion; and a frameshift Pro6Argfs*27 in two different tumors (Figure 4E). Furthermore, we identified two additional tumors with *NOTCH2* single copy deletion in 6/11 (54%) MECs with altered *NOTCH2* (Table S21). This *NOTCH* gene is known to play a role in adenoid cystic carcinoma tumorigenesis but has not previously been described in MEC tumors [42, 43]. Importantly, we also discovered a *TERT* His412Tyr missense mutation in one of 11 tumors (MEC 1), with a strong functional prediction score using functional annotation pipelines (Table S20). Given the prevalence of *TERT* promoter mutations in other cancers, we also evaluated *TERT* promoter status; however, no *TERT* promoter mutations were noted in any tumor (data not shown). We also identified copy number changes in several recurrently mutated genes (Figure 4F, Table S21), as well as *TERT* region focal amplification in several tumors (Figure 4G). In total, 5/11 (45%) MEC tumors contained a *TERT* mutation or copy number amplification. In addition, some recurrently copy number-altered genes, including *MUC5B and MAML1,* were also altered in MEC-derived cell lines (Figure S10).

Telomerase loss decreases survival of a TERT-rearranged Mucoepidermoid cell line model

As these data support recurrent *TERT* alterations in MEC, we sought to determine the functional importance of *TERT* in these tumors. Sanger sequencing validated *TERT* promoter mutation status in NCI-H292 and a set of HNSCC and sinonasal undifferentiated carcinoma (SNUC) models (Figure S11A). HNSCC cell lines UMSCC-47 and UMSCC-104, and SNUC cell line MDA8788–6, were selected as controls because they were found to have a wild-type *TERT* promoter. Telomere length of NCI-H292 was compared to UMSCC-47, UMSCC-104, and MDA8788–6. NCI-H292 cells displayed significantly longer telomeres than UMSCC-47, UMSCC-104, and MDA8788–6 cells, independent of passage number or patient age at the time of cell line creation (p=0.0005) (Figure S11B and Table S22).

To test the functional significance of *TERT* in MEC, we used publicly available DepMap CRISPR screen data [44], in which genome-wide CRISPR knockout screens were performed to define essential genes for survival in a panel of 342 cancer cell lines. We evaluated the importance of *TERT* relative to *MAML2* in NCI-H292 cell survival [45]. Previously published data have shown that *CRTC1::MAML2* expression is essential for NCI-H292 cell growth in vitro [9, 46]. We confirmed that *MAML2* gRNAs were identified in recently released depletion screens (CRISPR (Avana) Public 19Q3) [44]. Importantly, *MAML2* was highly essential for NCI-H292 survival (CERESscore = −0.83), but not for survival of most other cancer models, confirming a specific role for *MAML2* in mucoepidermoid cells (Figure 6A). As these data demonstrated that dropout CRISPR screening can effectively identify model-specific drivers, we explored the sensitivity to knockouts of genes with structural alterations identified above. While most of these genetically altered genes were not essential for NCI-H292 survival, *TERT* knockouts significantly affected NCI-H292 cell survival (CERESscore = −0.62). This response was in the top 2% of all profiled models. To validate these results, we transduced NCI-H292 and UM-SCC-104 cells with shRNA constructs targeting *TERT*. Consistent with the DepMap data, *TERT* knockdown caused significant reduction in clonogenic cell survival in NCI-H292, but not the control cells (Figure 6B-D), supporting the role of *TERT* as an essential driver in the *TERT*-rearranged cell line model.

Discussion

Multiple studies have shown the importance of *CRTC1::MAML2* fusion in MEC tumors and delineated mechanisms by which this fusion gene promotes tumorigenesis [12, 14–16], and until now, the molecular mechanism driving fusion formation has remained unresolved. Here, we provide the first evidence for a chain of five linked structural events resulting in the known (11;19)(q14–21; p12–13) or *CRTC1*::*MAML2* translocation. Our data demonstrate the involvement of *RP11554D151, VCPIP1* and *MYBL1* with the resultant rearrangement of *MYBL1.* While *MYBL1* translocation is known to play a role in acinic cell carcinoma tumorigenesis [12, 47], this is the first evidence of possible *MYBL1* involvement in MEC, suggesting a wider role in salivary gland malignancies. However, our exome cohort did not reveal additional *MYBL1* alterations; therefore, we chose not to pursue additional studies of the gene in MEC at this time. In contrast, our data revealed recurrent alterations predicted to activate *TERT* as well as alterations predicted to disrupt *NOTCH2* in MEC.

In head and neck malignancies, disruption of NOTCH signaling appears to be an important mechanism of pathogenesis [48]. Though some developmental studies suggest NOTCH signaling may play a role in salivary gland cell terminal fate decisions, the role of NOTCH receptors in mucoepidermoid carcinomas remains largely unknown [49, 50]. Furthermore, prior studies have shown that the *CRTC1::MAML2* fusion does not reproducibly alter NOTCH effector signaling. Notably, our data show *NOTCH2* receptor disruption in both *CRTC1::MAML2* fusion-positive and -negative tumors, supporting the hypothesis that NOTCH effector signaling acts independently from *MAML2* translocation in MEC. Although we were limited by a relatively small sample size due to the rarity of this disease, the high recurrence rate of *NOTCH2* alterations in our cohort suggests that the loss of

NOTCH2 is important in MEC progression, which may be critical for restricting cell fate decisions.

The role of *TERT* in mucoepidermoid carcinoma is limited in the literature[51]. However, there is evidence of a role of *TERT* in adenoid cystic carcinoma. A study by Morris *et al.* found that 14% (5/36) of adenoid cystic carcinoma samples harbored *TERT* promoter mutations [52]. In contrast, Kim *et al.* evaluated 36 benign and malignant salivary gland tumors, finding no samples containing *TERT* promoter mutations [53]. Further investigation into telomere length in parotid pleomorphic and carcinoma ex-pleomorphic adenoma tumors revealed increased relative telomere length in carcinoma ex-pleomorphic adenoma samples compared to pleomorphic adenomas or control samples. This was suggested to be secondary to alternative lengthening of telomeres driven by aberrant p14(ARF) and p16(INK4A) methylation, rather than increased telomerase activity [54]. Our data revealed two novel rearrangements involving the *TERT* promoter region in salivary MEC-derived cell lines. One of these cell lines, NCI-H292, demonstrated increased telomere length compared to other head and neck cancer cell lines, demonstrating a strong dependence of telomerase activity. Moreover, we detect translocations involving the *TERT* genomic locus in 39% (13/33) of MEC tumors by targeted capture sequencing, and translocations or copy number alterations in 92% (36/39) of MEC tumors by *TERT* break apart DNA FISH. These data represent some of the first evidence for a possible role of telomerase in MEC pathogenesis.

Finally, our data are the first to characterize full MEC genomes and support a high prevalence of structural rearrangements in this disease, especially when compared to concurrently profiled HNSCC models. In the future, larger cohort studies leveraging these genome sequencing approaches may lead to a better understanding of the frequency of rearrangement events in this disease, as well as the genetic mechanisms by which these rearrangements are formed. This is supported by our exome sequencing data from tumors, which suggest that MEC tumors have defects in homologous recombination-based DNA damage repair. Most importantly, while these data answer the longstanding question regarding the genetic mechanism of *CRTC1::MAML2* translocation, they also identify *TERT* as a possible novel driver of MEC. Given the ongoing efforts to develop telomerase-targeting therapeutic approaches for tumors with *TERT* aberrations, our discovery may have a significant impact on our basic understanding of MEC molecular oncogenesis, as well as the advancement of some of the first targeted therapy options for patients with this disease.

Supplementary Material

Refer to Web version on PubMed Central for supplementary material.

Acknowledgements

DNA sequencing of IHG-MUC360 was performed using the CePT Medical University of Warsaw infrastructure (Innovative Economy 2007-13, Agreement POIG.02.02.00-14-024/08-00). The VMP is a beneficiary of the START Program (2021) of the Foundation for Polish Science. Cell lines UM-HMC-1, UM-HMC-3A, and UM-HMC-3B were provided as a gift from the lab of Dr. Jacques Nör, in the University of Michigan School of Dentistry. Linked read sequencing, nanopore sequencing, RNA sequencing, whole exome sequencing, targeted capture sequencing was performed at the Advanced Genomics Core at the University of Michigan. FISH microscopy was performed at the University of Michigan Microscopy Core. Additional Sanger sequencing was performed at the RTSF Genomics Core at Michigan State University.

Funding

E.G. received funding from the National Institute of Health (NIH) (grant F31 DE030000-02). M. E. H. received funding from the NIH (grant T32 DC005356). This project was funded using start-up funds to J.C.B. from the University of Michigan

Data Availability Statement

Research data supporting this publication are available in the sequencing read archive repository at www.ncbi.nlm.nih.gov/sra. Any additional information required to reanalyze the data reported in this paper is available from the lead contact upon request.

References

[1]. Dombrowski ND, Wolter NE, Irace AL, Cunningham MJ, Mack JW, Marcus KJ, et al. Mucoepidermoid carcinoma of the head and neck in children. Int J Pediatr Otorhinolaryngol. 2019;120:93–9. [PubMed: 30772619]

[2]. Granic M, Suton P, Mueller D, Cvrljevic I, Luksic I. Prognostic factors in head and neck mucoepidermoid carcinoma: experience at a single institution based on 64 consecutive patients over a 28-year period. Int J Oral Maxillofac Surg. 2018;47:283–8. [PubMed: 28969884]

[3]. Nance MA, Seethala RR, Wang Y, Chiosea SI, Myers EN, Johnson JT, et al. Treatment and survival outcomes based on histologic grading in patients with head and neck mucoepidermoid carcinoma. Cancer. 2008;113:2082–9. [PubMed: 18720358]

[4]. Spiro RH. Salivary neoplasms: overview of a 35-year experience with 2,807 patients. Head Neck Surg. 1986;8:177–84. [PubMed: 3744850]

[5]. McHugh CH, Roberts DB, El-Naggar AK, Hanna EY, Garden AS, Kies MS, et al. Prognostic factors in mucoepidermoid carcinoma of the salivary glands. Cancer. 2012;118:3928–36. [PubMed: 22180391]

[6]. Byrd SA, Spector ME, Carey TE, Bradford CR, McHugh JB. Predictors of recurrence and survival for head and neck mucoepidermoid carcinoma. Otolaryngol Head Neck Surg. 2013;149:402–8. [PubMed: 23695589]

[7]. Birkeland AC, Foltin SK, Michmerhuizen NL, Hoesli RC, Rosko AJ, Byrd S, et al. Correlation of Crtc1/3-Maml2 fusion status, grade and survival in mucoepidermoid carcinoma. Oral Oncol. 2017;68:5–8. [PubMed: 28438292]

[8]. Chen J, Li JL, Chen Z, Griffin JD, Wu L. Gene expression profiling analysis of CRTC1-MAML2 fusion oncogene-induced transcriptional program in human mucoepidermoid carcinoma cells. BMC Cancer. 2015;15:803. [PubMed: 26503699]

[9]. Chen Z, Chen J, Gu Y, Hu C, Li JL, Lin S, et al. Aberrantly activated AREG-EGFR signaling is required for the growth and survival of CRTC1-MAML2 fusion-positive mucoepidermoid carcinoma cells. Oncogene. 2014;33:3869–77. [PubMed: 23975434]

[10]. Kang H, Tan M, Bishop JA, Jones S, Sausen M, Ha PK, et al. Whole-Exome Sequencing of Salivary Gland Mucoepidermoid Carcinoma. Clinical cancer research : an official journal of the American Association for Cancer Research. 2017;23:283–8. [PubMed: 27340278]

[11]. Shinomiya H, Ito Y, Kubo M, Yonezawa K, Otsuki N, Iwae S, et al. Expression of amphiregulin in mucoepidermoid carcinoma of the major salivary glands: a molecular and clinicopathological study. Hum Pathol. 2016;57:37–44. [PubMed: 27393417]

[12]. Yan K, Yesensky J, Hasina R, Agrawal N. Genomics of mucoepidermoid and adenoid cystic carcinomas. Laryngoscope investigative otolaryngology. 2018;3:56–61. [PubMed: 29492469]

[13]. Toper MH, Sarioglu S. Molecular Pathology of Salivary Gland Neoplasms: Diagnostic, Prognostic, and Predictive Perspective. Adv Anat Pathol. 2021;28:81–93. [PubMed: 33405400]

[14]. Behboudi A, Enlund F, Winnes M, Andren Y, Nordkvist A, Leivo I, et al. Molecular classification of mucoepidermoid carcinomas-prognostic significance of the MECT1-MAML2 fusion oncogene. Genes Chromosomes Cancer. 2006;45:470–81. [PubMed: 16444749]

[15]. Komiya T, Park Y, Modi S, Coxon AB, Oh H, Kaye FJ. Sustained expression of Mect1-Maml2 is essential for tumor cell growth in salivary gland cancers carrying the t(11;19) translocation. Oncogene. 2006;25:6128–32. [PubMed: 16652146]

[16]. Tonon G, Modi S, Wu L, Kubo A, Coxon AB, Komiya T, et al. t(11;19)(q21;p13) translocation in mucoepidermoid carcinoma creates a novel fusion product that disrupts a Notch signaling pathway. Nat Genet. 2003;33:208–13. [PubMed: 12539049]

[17]. Okumura Y, Miyabe S, Nakayama T, Fujiyoshi Y, Hattori H, Shimozato K, et al. Impact of CRTC1/3-MAML2 fusions on histological classification and prognosis of mucoepidermoid carcinoma. Histopathology. 2011;59:90–7. [PubMed: 21668476]

[18]. Nakayama T, Miyabe S, Okabe M, Sakuma H, Ijichi K, Hasegawa Y, et al. Clinicopathological significance of the CRTC3-MAML2 fusion transcript in mucoepidermoid carcinoma. Mod Pathol. 2009;22:1575–81. [PubMed: 19749740]

[19]. Guerrero-Preston R, Godoy-Vitorino F, Jedlicka A, Rodriguez-Hilario A, Gonzalez H, Bondy J, et al. 16S rRNA amplicon sequencing identifies microbiota associated with oral cancer, human papilloma virus infection and surgical treatment. Oncotarget. 2016;7:51320–34. [PubMed: 27259999]

[20]. Coxon A, Rozenblum E, Park YS, Joshi N, Tsurutani J, Dennis PA, et al. Mect1-Maml2 fusion oncogene linked to the aberrant activation of cyclic AMP/CREB regulated genes. Cancer Res. 2005;65:7137–44. [PubMed: 16103063]

[21]. Wu L, Liu J, Gao P, Nakamura M, Cao Y, Shen H, et al. Transforming activity of MECT1-MAML2 fusion oncoprotein is mediated by constitutive CREB activation. EMBO J. 2005;24:2391–402. [PubMed: 15961999]

[22]. Amelio AL, Fallahi M, Schaub FX, Zhang M, Lawani MB, Alperstein AS, et al. CRTC1/MAML2 gain-of-function interactions with MYC create a gene signature predictive of cancers with CREB-MYC involvement. Proc Natl Acad Sci U S A. 2014;111:E3260–8. [PubMed: 25071166]

[23]. Musicant AM, Parag-Sharma K, Gong W, Sengupta M, Chatterjee A, Henry EC, et al. CRTC1/MAML2 directs a PGC-1alpha-IGF-1 circuit that confers vulnerability to PPARgamma inhibition. Cell Rep. 2021;34:108768.

[24]. Kar A, Adeniji A, Rao VUS, Ghosh M. Molecular landscape of salivary gland cancers. Oral Oncol. 2020:104595.

[25]. Brenner JC, Graham MP, Kumar B, Saunders LM, Kupfer R, Lyons RH, et al. Genotyping of 73 UM-SCC head and neck squamous cell carcinoma cell lines. Head & neck. 2010;32:417–26. [PubMed: 19760794]

[26]. Warner KA, Adams A, Bernardi L, Nor C, Finkel KA, Zhang Z, et al. Characterization of tumorigenic cell lines from the recurrence and lymph node metastasis of a human salivary mucoepidermoid carcinoma. Oral Oncol. 2013;49:1059–66. [PubMed: 24035723]

[27]. Takahashi Y, Lee J, Pickering C, Bell D, Jiffar TW, Myers JN, et al. Human epidermal growth factor receptor 2/neu as a novel therapeutic target in sinonasal undifferentiated carcinoma. Head & neck. 2016;38 Suppl 1:E1926–34.

[28]. Ludwig ML, Kulkarni A, Birkeland AC, Michmerhuizen NL, Foltin SK, Mann JE, et al. The genomic landscape of UM-SCC oral cavity squamous cell carcinoma cell lines. Oral Oncol. 2018;87:144–51. [PubMed: 30527230]

[29]. Li Y, Roberts ND, Wala JA, Shapira O, Schumacher SE, Kumar K, et al. Patterns of somatic structural variation in human cancer genomes. Nature. 2020;578:112–21. [PubMed: 32025012]

[30]. Ordulu Z, Wong KE, Currall BB, Ivanov AR, Pereira S, Althari S, et al. Describing sequencing results of structural chromosome rearrangements with a suggested next-generation cytogenetic nomenclature. Am J Hum Genet. 2014;94:695–709. [PubMed: 24746958]

[31]. van Weert S, Lissenberg-Witte BI, Bloemena E, Leemans CR. Mucoepidermoid carcinoma of the head and neck: CRTC1/3 MAML 2 translocation and its prognosticators. Eur Arch Otorhinolaryngol. 2022;279:2573–81. [PubMed: 34405264]

[32]. Perez-de-Oliveira ME, Wagner VP, Araujo ALD, Martins MD, Santos-Silva AR, Bingle L, et al. Prognostic value of CRTC1-MAML2 translocation in salivary mucoepidermoid carcinoma: Systematic review and meta-analysis. J Oral Pathol Med. 2020;49:386–94. [PubMed: 31661572]

[33]. Okumura Y, Nakano S, Murase T, Ueda K, Kawakita D, Nagao T, et al. Prognostic impact of CRTC1/3-MAML2 fusions in salivary gland mucoepidermoid carcinoma: A multiinstitutional retrospective study. Cancer Sci. 2020;111:4195–204. [PubMed: 32860299]

[34]. Cleal K, Baird DM. Dysgu: efficient structural variant calling using short or long reads. Nucleic Acids Res. 2022;50:e53. [PubMed: 35100420]

[35]. Blokzijl F, Janssen R, van Boxtel R, Cuppen E. MutationalPatterns: comprehensive genome-wide analysis of mutational processes. Genome Med. 2018;10:33. [PubMed: 29695279]

[36]. Tate JG, Bamford S, Jubb HC, Sondka Z, Beare DM, Bindal N, et al. COSMIC: the Catalogue Of Somatic Mutations In Cancer. Nucleic Acids Research. 2018;47:D941–D7.

[37]. Alexandrov LB, Nik-Zainal S, Wedge DC, Aparicio SA, Behjati S, Biankin AV, et al. Signatures of mutational processes in human cancer. Nature. 2013;500:415–21. [PubMed: 23945592]

[38]. Jiang Z, Wang H, Li L, Hou Z, Liu W, Zhou T, et al. Analysis of TGCA data reveals genetic and epigenetic changes and biological function of MUC family genes in colorectal cancer. Future Oncol. 2019;15:4031–43. [PubMed: 31773991]

[39]. Wang J, Zhou H, Wang Y, Huang H, Yang J, Gu W, et al. Serum mucin 3A as a potential biomarker for extrahepatic cholangiocarcinoma. Saudi J Gastroenterol. 2020;26:129–36. [PubMed: 32270773]

[40]. Honjo K, Hiraki T, Higashi M, Noguchi H, Nomoto M, Yoshimura T, et al. Immunohistochemical expression profiles of mucin antigens in salivary gland mucoepidermoid carcinoma: MUC4- and MUC6-negative expression predicts a shortened survival in the early postoperative phase. Histol Histopathol. 2018;33:201–13. [PubMed: 28649694]

[41]. Robinson L, van Heerden MB, Ker-Fox JG, Hunter KD, van Heerden WFP. Expression of Mucins in Salivary Gland Mucoepidermoid Carcinoma. Head Neck Pathol. 2020.

[42]. Bell D, Hanna EY, Miele L, Roberts D, Weber RS, El-Naggar AK. Expression and significance of notch signaling pathway in salivary adenoid cystic carcinoma. Ann Diagn Pathol. 2014;18:10–3. [PubMed: 24238845]

[43]. Ding LC, She L, Zheng DL, Huang QL, Wang JF, Zheng FF, et al. Notch-4 contributes to the metastasis of salivary adenoid cystic carcinoma. Oncol Rep. 2010;24:363–8. [PubMed: 20596622]

[44]. Meyers RM, Bryan JG, McFarland JM, Weir BA, Sizemore AE, Xu H, et al. Computational correction of copy number effect improves specificity of CRISPR-Cas9 essentiality screens in cancer cells. Nat Genet. 2017;49:1779–84. [PubMed: 29083409]

[45]. DepMap BDQPfDdmfv.

[46]. Chen Z, Lin S, Li JL, Ni W, Guo R, Lu J, et al. CRTC1-MAML2 fusion-induced lncRNA LINC00473 expression maintains the growth and survival of human mucoepidermoid carcinoma cells. Oncogene. 2018;37:1885–95. [PubMed: 29353885]

[47]. Persson M, Andren Y, Mark J, Horlings HM, Persson F, Stenman G. Recurrent fusion of MYB and NFIB transcription factor genes in carcinomas of the breast and head and neck. Proc Natl Acad Sci U S A. 2009;106:18740–4. [PubMed: 19841262]

[48]. Cancer Genome Atlas N. Comprehensive genomic characterization of head and neck squamous cell carcinomas. Nature. 2015;517:576–82. [PubMed: 25631445]

[49]. Haberman AS, Isaac DD, Andrew DJ. Specification of cell fates within the salivary gland primordium. Dev Biol. 2003;258:443–53. [PubMed: 12798300]

[50]. Dang H, Lin AL, Zhang B, Zhang HM, Katz MS, Yeh CK. Role for Notch signaling in salivary acinar cell growth and differentiation. Dev Dyn. 2009;238:724–31. [PubMed: 19235730]

[51]. Shigeishi H, Sugiyama M, Tahara H, Ono S, Kumar Bhawal U, Okura M, et al. Increased telomerase activity and hTERT expression in human salivary gland carcinomas. Oncol Lett. 2011;2:845–50. [PubMed: 22866138]

[52]. Morris LGT, Chandramohan R, West L, Zehir A, Chakravarty D, Pfister DG, et al. The Molecular Landscape of Recurrent and Metastatic Head and Neck Cancers: Insights From a Precision Oncology Sequencing Platform. JAMA Oncol. 2017;3:244–55. [PubMed: 27442865]

[53]. Kim H, Ahn D, Sohn JH, Kim YH, Lee JH, Lee H. TERT Promoter Mutation and Telomere Length in Salivary Gland Tumors. Pathol Oncol Res. 2018;24:697–8. [PubMed: 28664476]

[54]. Nikolic N, Anicic B, Carkic J, Simonovic J, Toljic B, Tanic N, et al. High frequency of p16 and p14 promoter hypermethylation and marked telomere instability in salivary gland tumors. Archives of oral biology. 2015;60:1662–6. [PubMed: 26351750]

[55]. Ghandi M, Huang FW, Jane-Valbuena J, Kryukov GV, Lo CC, McDonald ER 3rd, et al. Next-generation characterization of the Cancer Cell Line Encyclopedia. Nature. 2019;569:503–8. [PubMed: 31068700]

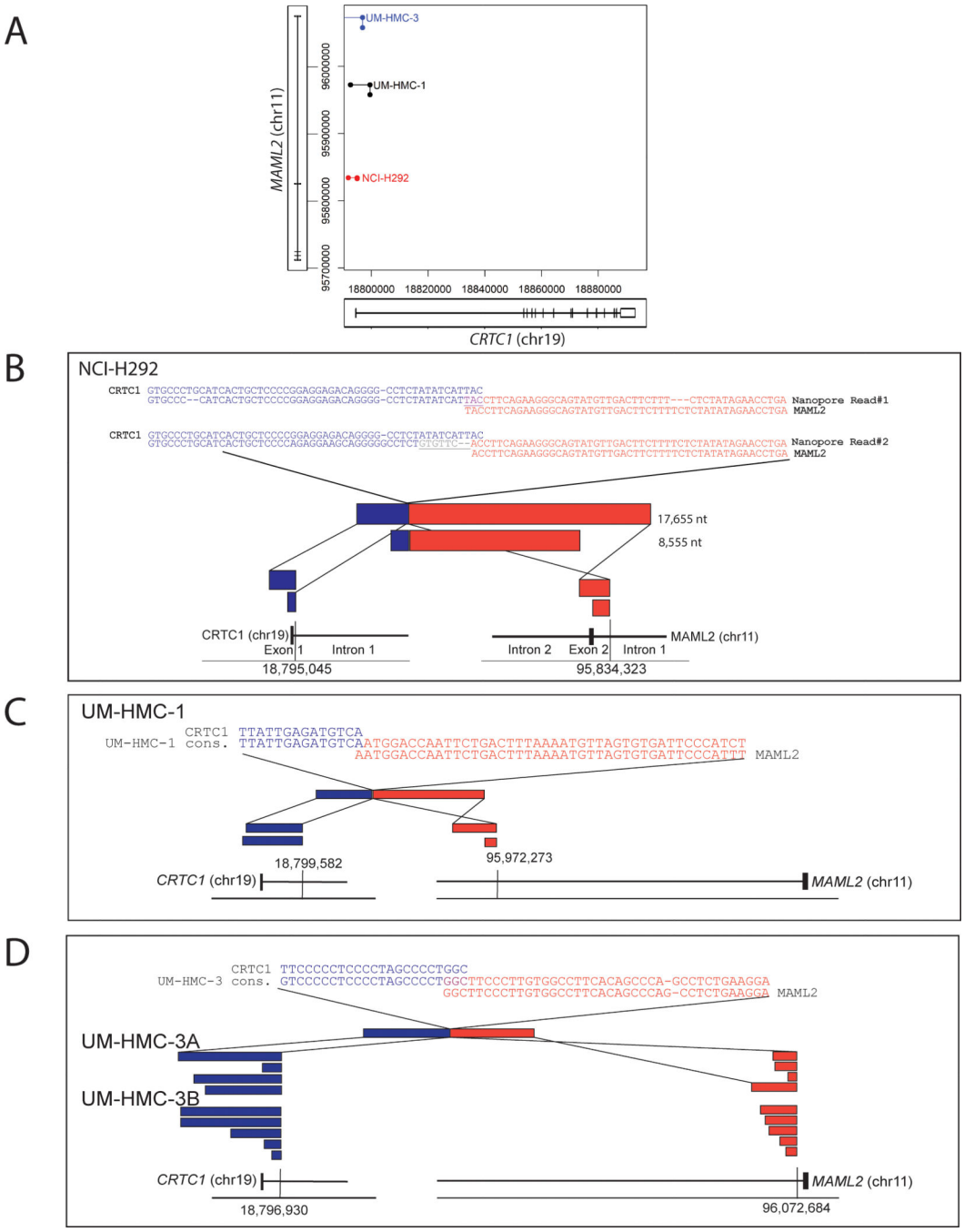

Figure 1. *CRTC1::MAML2* breakpoint is directly sequenced by long read Nanopore DNA sequencing.

A) Coordinates of reads split between both CRTC1 and MAML2 for each cell line sequenced. UM-HMC-3A and UM-HMC-3B share a genetic background, so are recorded as UM-HMC-3. **B)** Schematic represents independent reads that identify the CRTC1::MAML2 breakpoint in NCI-H292, **C)** UM-HMC-1, **D)** UM-HMC-3A, and UM-HMC-3B. Consensus sequences of each breakpoint are shown.

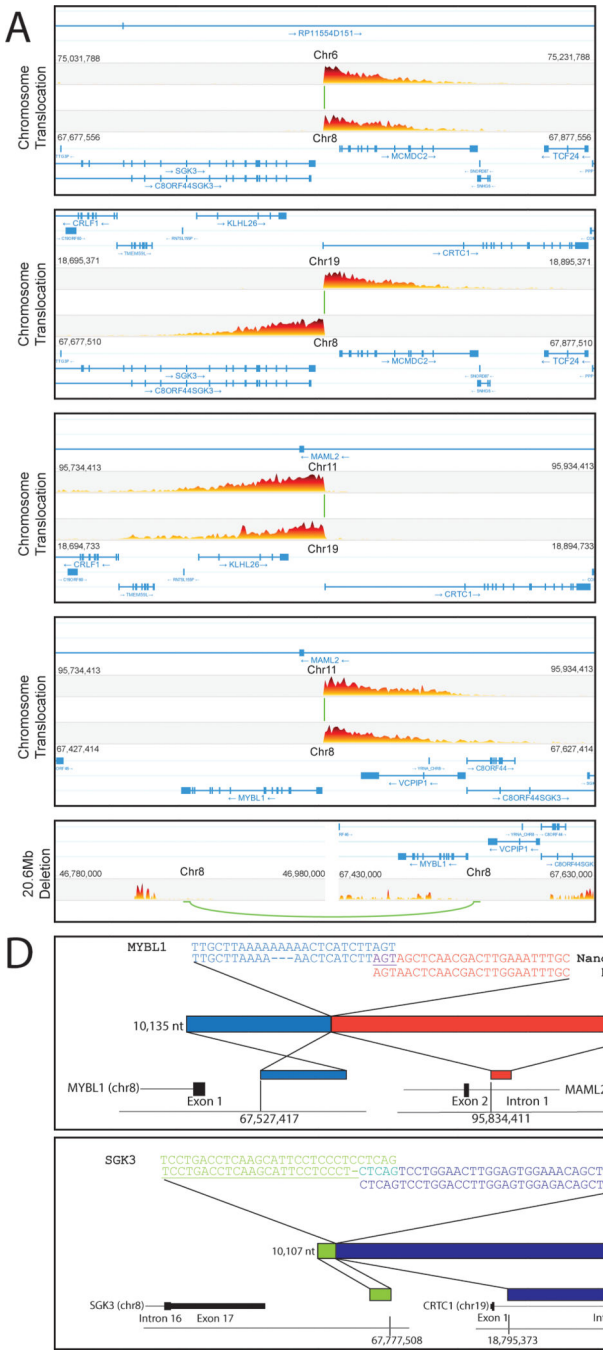

NIH-H292		
Chromosome	**Nucleotide**	**Gene**
Chr1	203,790,176	*ZC3H11A*
Chr16	75,654,182	*ADAT1*
Chr11	128,914,826	*ARHGAP32*
Chr7	96,079,993	-
Chr11	129,180,323	*ARHGAP32*
Chr13	27,111,074	*WASF3*
Chr11	123,296,777	-
Chr5	1,535,777	-
Chr11	95,834,411	*MAML2*
Chr8	67,527,412	*MYBL1*
Chr19	18,795,369	*CRTC1*
Chr8	67,777,508	*SGK3*
Chr6	75,131,786	*RP11554D151*
Chr8	67,777,554	*MCMDC2*
Chr11	95,834,323	*MAML2*
Chr19	18,794,730	*CRTC1*
Chr11	111,600,986	*PPP2R1B*
Chr5	1,296,648	*TERT*

Figure 2. Linked Read Sequencing Resolves the Genetic Mechanism Driving *CRTC1::MAML2* Rearrangement in the NCI-H292 Mucoepidermoid Carcinoma Cell Line.

A) Five structural variations were discovered in NCI-H292, associated with the *CRTC1* to *MAML2* genomic rearrangement. Structures of individual events are shown. **B)** High confidence chromosomal rearrangements and estimated genomic breakpoints discovered in NCI-H292. **C)** Schematic representation shows independent reads used to identify the *MYBL1* to *MAML2* translocation, and the *SGK3* to *CRTC1* translocation. GRCh37/hg19 coordinates are shown, with sequences spanning the breakpoint annotated at the top of the

figure **D)** Genome-wide view of the chained structural events leading to the *CRTC1* to *MAML2* translocation.

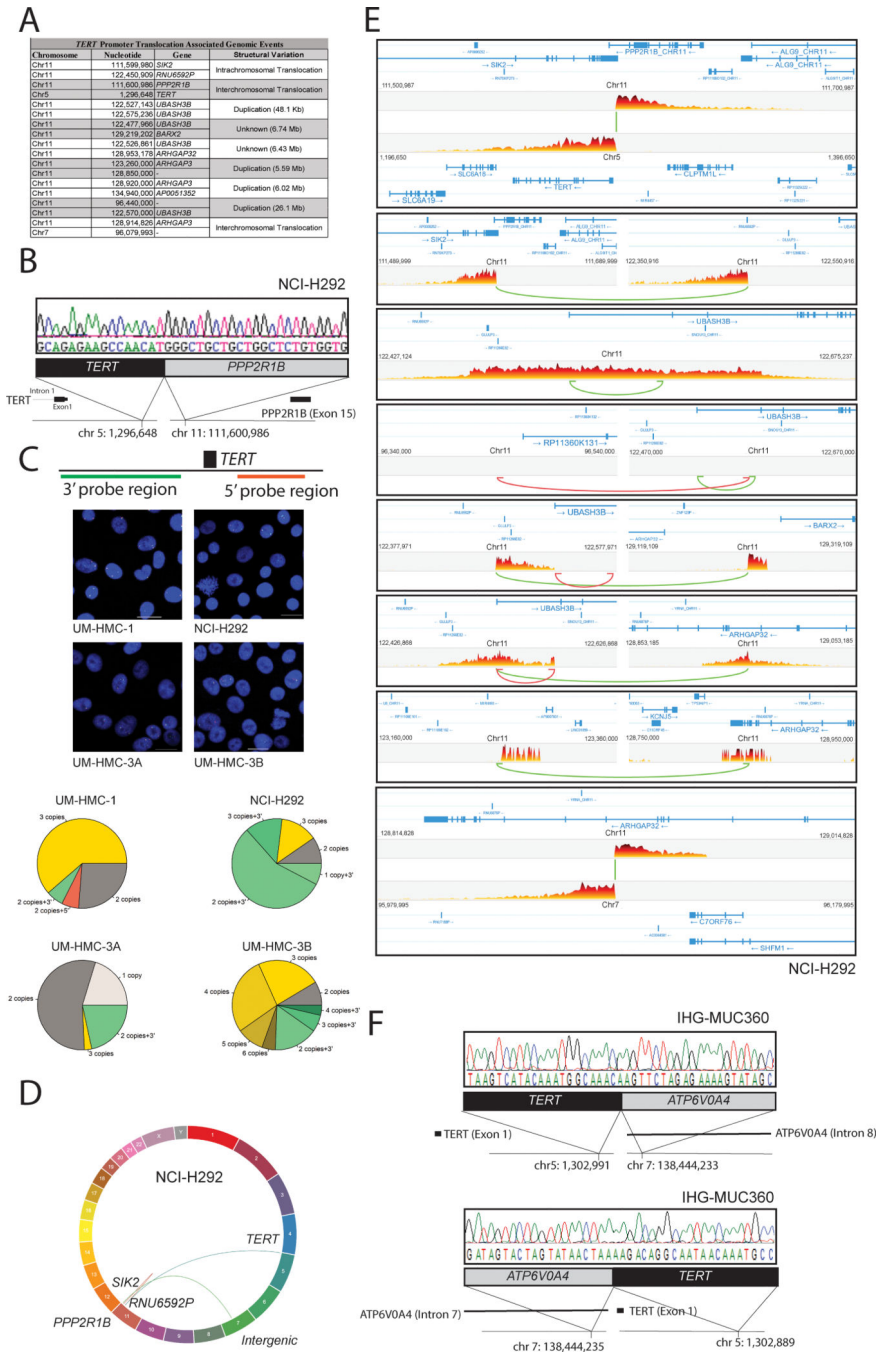

Figure 3. Discovery and Validation of Recurrent Structural Variation at the TERT Promoter in MEC.

A) The coordinates for the nine linked high and low confidence structural events associated with a structural rearrangement in which the 5' region of the *PPP2R1B* gene is rearranged to replace the *TERT* promoter in NCI-H292 are listed. Additional structural variations to Chr11 include potential deletions and duplications of *UBASH3B*, *ARHGAP32*, and the *BARX2* genes as well as translocation of *ARHGAP3* and *SIK2*. Linked read estimated breakpoints are shown. **B)** Sanger sequencing was used to validate the *PPP2R1B* to *TERT*

rearrangement breakpoint in NCI-H292 **C)** *TERT* locus visualized by FISH with *TERT* break apart probe with orange (5-TAMRA) fluorophore adjacent to the 5' region of *TERT* and green (5-Fluoresceine) fluorophore adjacent to the 3' region (schematic top panel). Nucleus is blue (DAPI). Scale bar=20 μm. Right panel shows quantification of *TERT* locus FISH, N>50 cells per cell line. **D)** Genome-wide view of the chained structural events leading to the *PPP2R1B* to *TERT* translocation, **E)** Structure of individual breakpoint events in NCI-H292, identified by linked read sequencing. **F)** Sanger sequencing presenting the chromosome der(5) (left) and chromosome der(7) (right) junction at single base pair resolution of the TERT rearrangement identified in the IHG-360 MEC cell line.

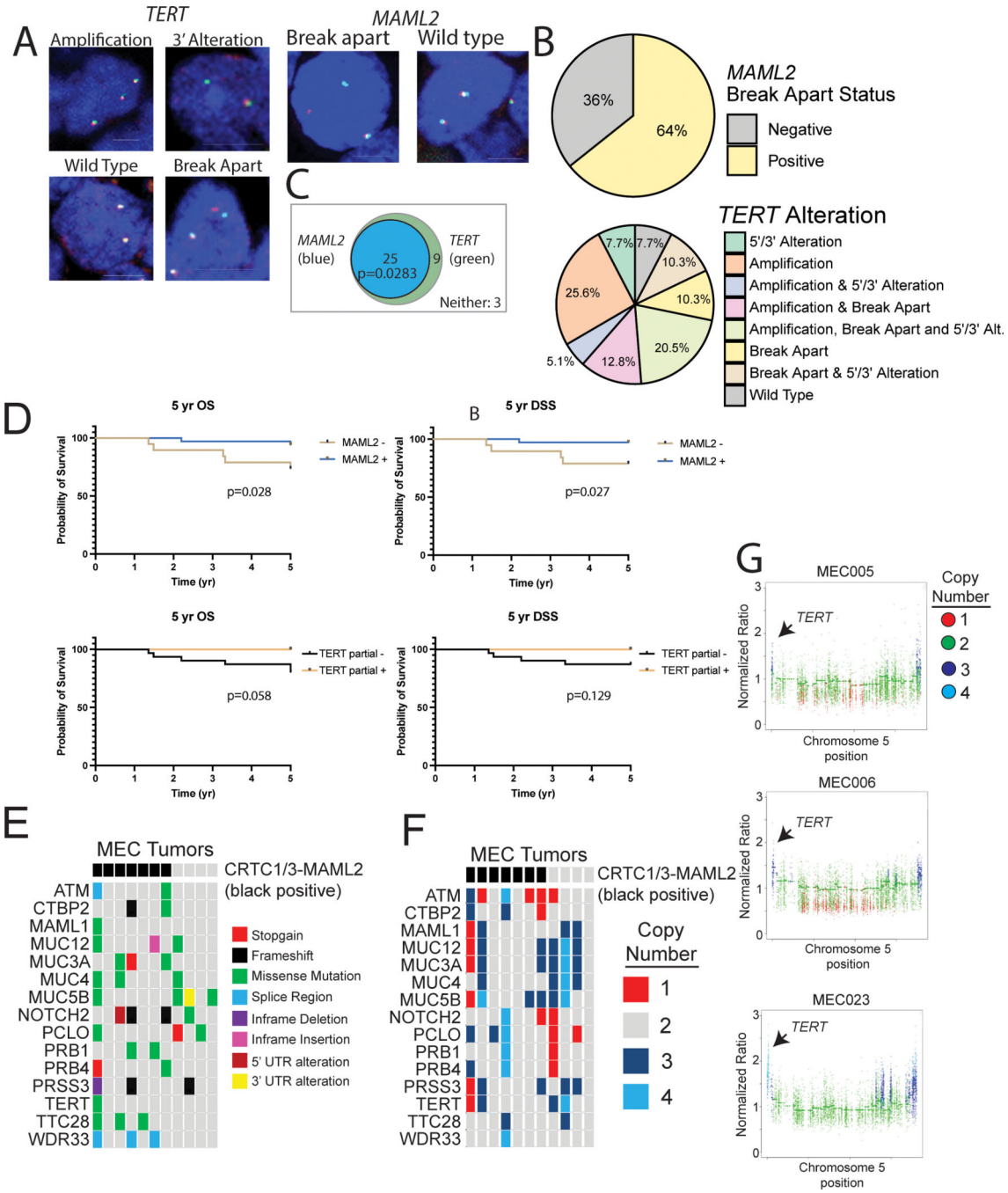

Figure 4. MAML2 and TERT structural variation detected by FISH.

A) Representative images of each structural variant. Nuclei are stained with DAPI (blue). *MAML2* break apart is characterized by an orange (5-TAMRA, 5') puncta separated from a green (5-Fluorescein, 3') puncta. For the second copy of *MAML2*, the 5' and 3' signal overlap, indicating a wild-type structure. *TERT* variants include amplification, break apart, and 5'/3' alteration (bar=5 micron). Wild type and break apart punctae are characterized as with *MAML2.* Amplification is characterized by more than 2 wild type punctae in a single cell, or two wild type punctae if a break apart is present and represents the presence of either

a focal *TERT* amplicon or a larger amplicon from the 5p region containing the *TERT* gene. *TERT* break apart is characterized by separated orange (5') and green (3') punctae. 5' or 3' alteration is characterized by a single orange (5') or green (3') signal, without the other color also being present. Due to the frequency of *TERT* amplification, the same event could be described as a 3' amplification or a 5' deletion, which is why the descriptor "alteration" was chosen. **B)** Proportion of tumors containing each kind of *MAML2* (top, N=56) or *TERT* (bottom, N=49) structural variation. Scale bar=5μm. **C)** Overlap between tumors containing *MAML2* and *TERT* structural variants. There is significant overlap between tumors containing mutations in each gene (Fisher's exact test, p=0.0283) **D)** Kaplan-Meier survival analysis shows that presence of *MAML2*, but not *TERT*, structural variants are associated with increased disease-specific survival (DSS) and overall survival (OS). **E**) Oncoplot highlighting recurrent single nucleotide variants and insertions/deletions (INDELs) in the cohort. *CRTC1/3::MAML2* fusion status of each tumor is shown in the top bar. **F)** Copy number annotation of each of the highlighted genes from panel C, along with *CRTC1/3::MAML2* fusion status. **G)** Representative Manhattan plots of Chromosome 5 from the three tumors with called focal *TERT* amplification.

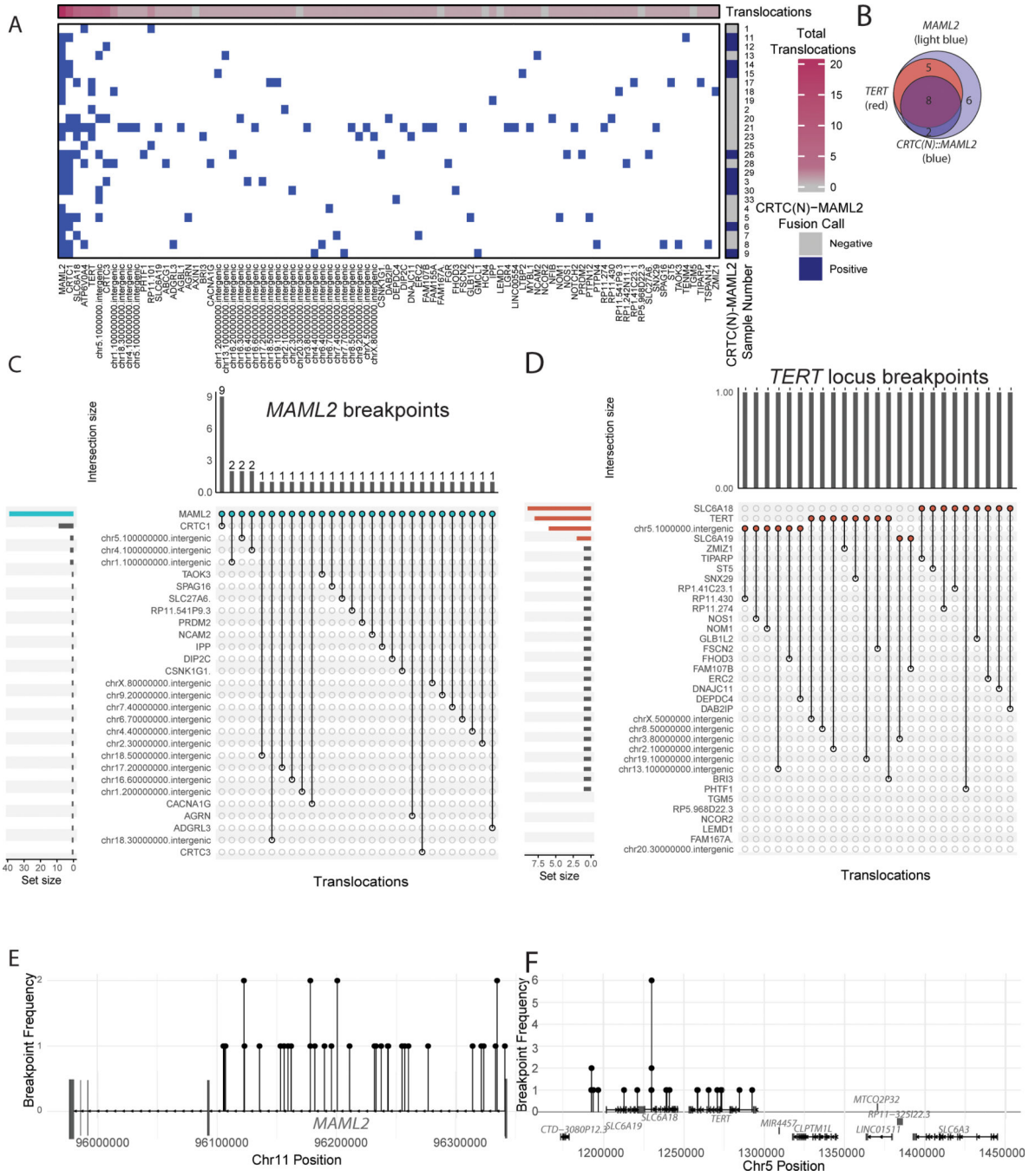

Figure 5. Translocations identified by targeted capture sequencing.

A) Genes and intergenic regions associated with a called translocation. 26/33 samples contain one or more translocations captured by the targeted panel, and are pictured. **B)** Venn diagram of samples containing *TERT* (red) and *MAML2* (blue) translocations. Translocations involving either locus were not detected in 12/33 samples. There is significant overlap between *TERT* and *MAML2* translocations (Fisher's exact test p=0.0005). **C)** Translocations associated with *MAML2* (blue). **D)** Translocations associated with genes and the intergenic region within the genomic locus flanking *TERT* by 50,000

base pairs (red). **E-F)** genomic positions of breakpoints associated with **E)** MAML2 and **F)** *TERT* genetic loci.

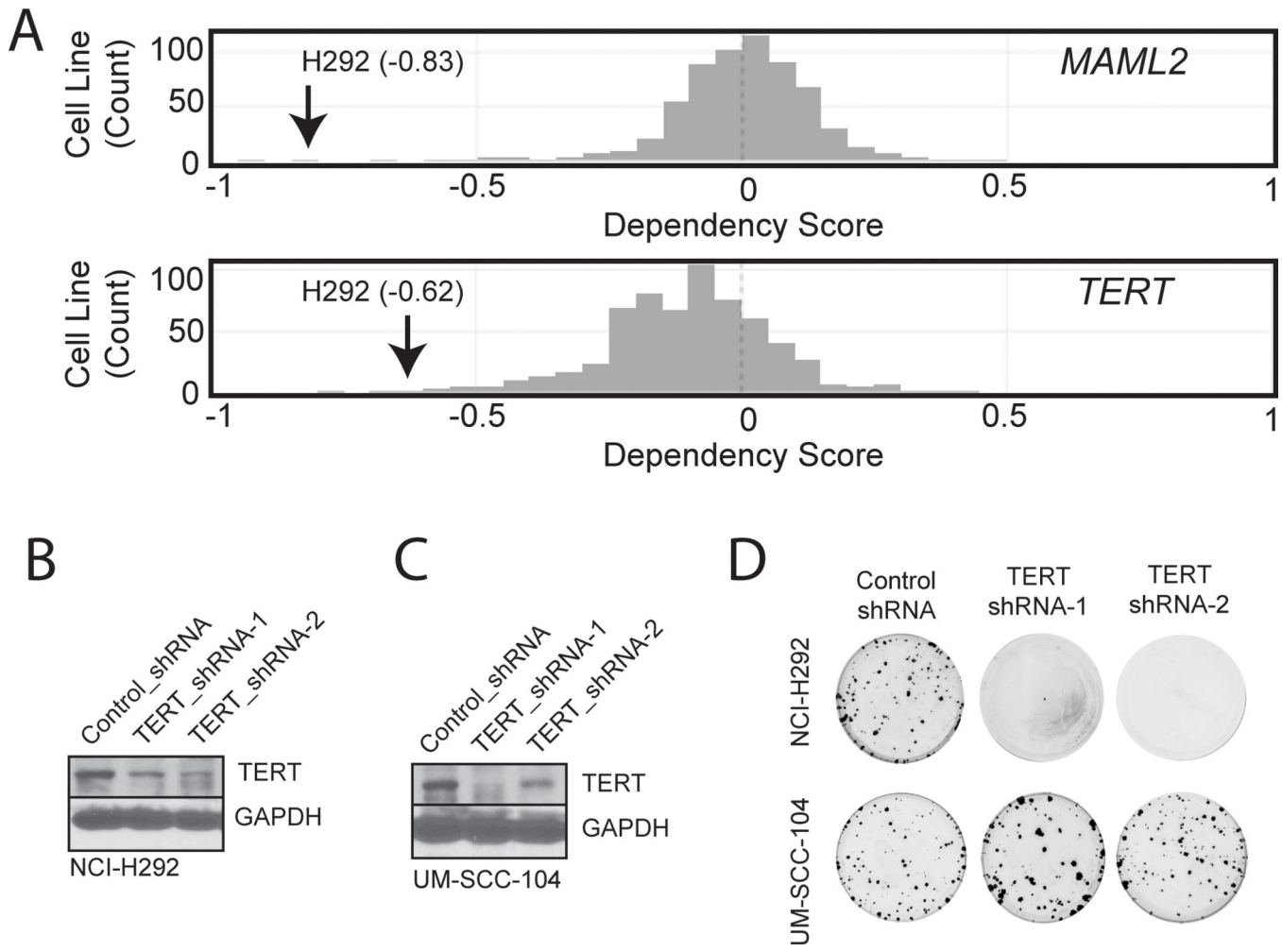

Figure 6. Functional Evaluation of the Role of TERT in NCI-H292.

A) Dependency Score. The CERESdepletion score was based on data from a depletion assay. A lower CERESscore indicates a higher likelihood that the gene is essential in each cell line. A score of zero indicates that a gene is not essential, and a score of −1 is comparable to the median of all pan-essential genes. Dropout CRISPR screening data were downloaded from the Avana 19Q3 public release. *MAML2* and *TERT* are essential for survival in NCI-H292. **B and C)** *TERT* shRNA was used to infect NCI-H292 or UM-SCC-104 cells, and changes in telomerase protein expression were detected by Western blot. **D)** Cells from D & E were re-plated into clonogenic cell survival assays after 48 hours and grown in culture in parallel for >10 days, at which point plates were imaged to show relative colony formation for each condition.